

Modeling tree topology effects on wind (P2)

Runnan Fu



1st supervisor: Clara García-Sánchez

2nd supervisor: Ivan Pađen

January, 2022

1 Introduction

1.1 Motivation

With more and more people living in urban areas, urbanisation is expanding. The rise of human activities is linked to problems such as the rising temperatures (Urban Heat Islands (UHI), specially at night) and air pollution in cities, which eventually can lead to various human diseases and premature deaths (Fouillet et al., 2006; Salmond et al., 2016). Since a good urban wind environment can ameliorate air quality, mitigate heat island effects, improve pedestrian wind comfort and reduce buildings energy consumption, this field of research is currently receiving more and more attention (Hsieh and Huang, 2016; Blocken et al., 2012).

A widely considered economical and effective way to create a good urban wind environment is planting of trees (Salmond et al., 2016; Aflaki et al., 2017; Szkordilisz and Zöld, 2016), as trees can affect the wind flow by reducing its speed and changing its direction (Szkordilisz and Zöld, 2016). It is worth noting that the dynamic effects of trees on urban wind environment depends not only on environmental factors such as the surrounding built environment, local climate and wind speed, but also on tree properties such as tree shape, height and foliage density (Hefny Salim et al., 2015; Manickathan et al., 2018). In order to assess tree effect and find suitable tree setups in urban areas, numerical simulations can be used.

However, for practical purposes and lack of information, the geometric features of trees are usually ignored in numerical simulations of the wind flow in urban areas. To handle trees, the porosity parametrization approach is widely used where finite volume cells that roughly account for trees are marked as porous zones (Hefny Salim et al., 2015; Kang et al., 2020). In these porous zones, the effect of trees is defined as a source and/or sink term in the momentum equation and turbulence equations. It can be seen that this approach models trees implicitly, which overlooks resolving tree structures. However, the influence of tree canopy, trunk and branches on flow structure cannot be ignored. (Hong et al., 2018b) demonstrated that wind slows down significantly at branches, and that the wind velocity distribution in tree canopy is not uniform and depends heavily on the location of branches. Therefore, an explicit approach, i.e., geometric modeling of the tree topology in numerical simulations, is worth studying. In this context, the questions arise: to what extent can we represent the tree effect implicitly, and can we live with that compromise? what is the percentage error comparing the implicit and the explicit approaches?

1.2 Objectives

The goals of this thesis is to explicitly model diverse tree topology, and analyze the impact of different tree shapes on the flow structure. The insights gathered will be used to evaluate the performance of traditional drag approaches and explore the potential improvements in implicit tree modelling using the explicit tree models as a reference.

2 Related work

In this section, the theory and literature related to flow simulations and tree modeling is discussed. First, a general background of urban wind flows is given. After that, the numerical

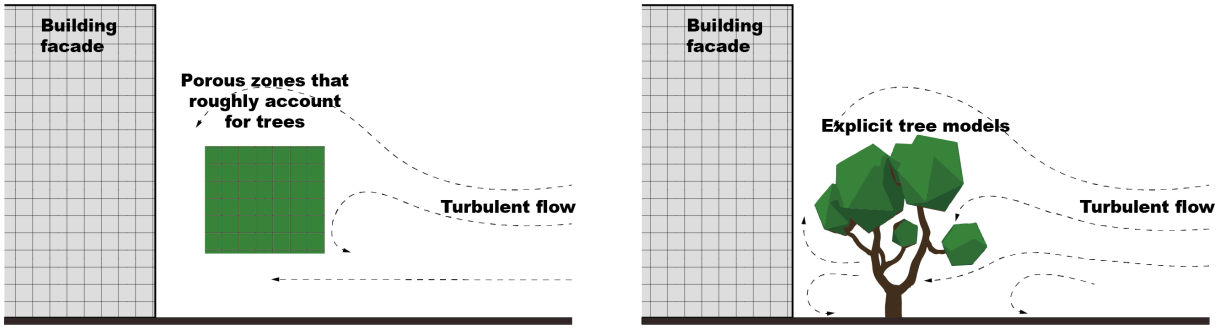


Figure 1.1: Abstract representation of the research objectives

models and implicit tree modeling approach currently used to conduct flow simulations are discussed. The development of 3D tree modeling is also presented, which is useful for this thesis to find an explicit tree modeling approach suitable for urban wind flow simulations.

2.1 Urban wind flows

As an atmospheric phenomenon, winds occur in a range of spatial and temporal dimensions, from a few tens of meters to thousands of kilometers, and from seconds to weeks (figure 2.1). In general, they can be grouped into three different scale categories (Blocken, 2015):

1. Macroscale or synoptic scale: includes phenomena such as migrating cyclones that control daily weather changes, ranging from a few hundred to a few thousand kilometres.
2. Mesoscale: includes phenomena such as mountain waves, sea and land breezes, thunderstorms, which range from a dozen to several hundred kilometres and have a lifetime of one day or less.
3. Microscale: includes phenomena such as building wakes and turbulence, which have spatial scales of 2 km or less.

In the field of built environment, research is mainly focused on the meteorological microscale and building scale. At these scales, in order to understand the transport and distribution of fluids, such as wind or pollutants, three methods can be used: 1) field measurements 2) wind tunnel measurements, and 3) numerical simulation methods, mainly Computational Fluid Dynamics (CFD) (Blocken, 2015).

The fundamental consideration of CFD is how to deal with continuous fluids in a discrete manner on a computer. One approach is to discretize the computational domain into finite volumes (figure 2.2), and then apply suitable algorithms to solve the transport equations such as mass, momentum, and energy equations for each finite volume. The general formulation of the transport equations for compressible flow in differential form (Moukalled et al., 2016) is

$$\frac{\partial}{\partial t}(\rho\phi) + \nabla \cdot (\rho\mathbf{v}\phi) = \nabla \cdot (\Gamma^\phi \nabla \phi) + Q^\phi \quad (1)$$

where the four components, from left to right, are unsteady term, convection term, diffusion term and source/sink term; ρ is the fluid density, ϕ is the quantity of interest, \mathbf{v} is velocity, Γ is the diffusion coefficient and Q^ϕ is the generation/destruction of ϕ within the control volume per unit volume.

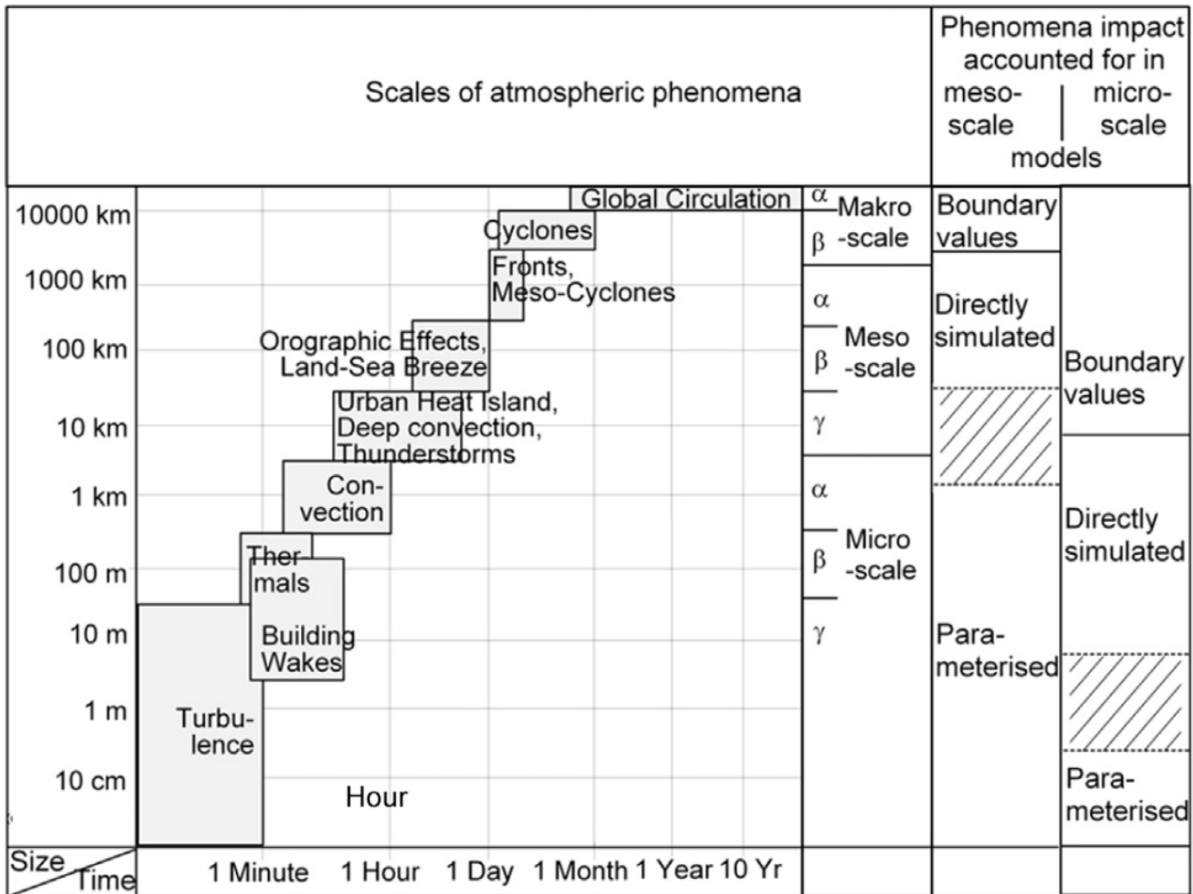


Figure 2.1: Spatial and temporal scales of atmospheric phenomena (Source: Blocken, 2015)

The computational mesh is one of the key aspects to accurate CFD predictions. A high quality computational mesh not only reduces discretization errors, but also promotes convergence (Blocken, 2015; Tominaga et al., 2008). It is worth noting that complex meshes may lead to a decrease in mesh quality and a significant increase in the number of mesh cells, resulting in errors and long processing times. However, computational meshes are often complex due to the presence of complicated 3D geometries, such as buildings and trees with detailed features. Therefore, an acceptable degree of simplification of geometries in CFD simulations is recommended (Tominaga et al., 2008). Such simplifications include using parameters in place of geometry, for example, using porosity or roughness length, or adding additional terms in the transport equations. In addition, reducing the Level of Detail (LoD) of geometric objects and removing small geometric features are also common simplifications. Indeed, simplifications may affect simulation results and introduce some uncertainty, so finding an acceptable level of simplification and investigating the effect of LoDs on urban wind flow simulations will also be goals of this work.

2.2 Current numerical simulations of tree effects on wind

There has been a lot of interest in using CFD models to study tree effects. Current studies have focused on the effects on air quality (Vos et al., 2013; Santiago et al., 2019; Balczó et al., 2009; Moradpour et al., 2017), pedestrian wind comfort (Kang et al., 2020; Hong and Lin, 2015) and thermal urban environment (Manickathan et al., 2018; Hong and Lin, 2015; Gromke et al.,

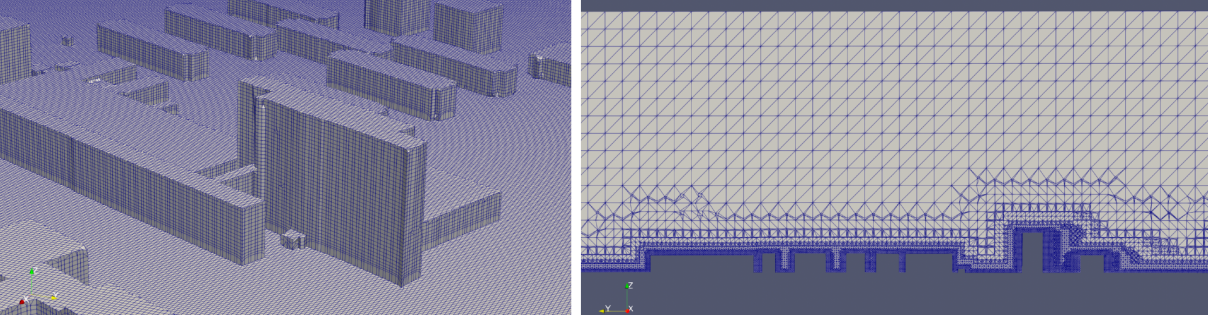


Figure 2.2: Finite volume mesh for a 3D city model

2015). Although the above numerical simulation studies have demonstrated the importance of trees, in these studies trees were usually reduced to circular or rectangular porous zones (figure 2.3) rather than geometrically modeled as objects. That is, these studies have chosen to implicitly model trees. This is mainly due to the fact that such implicit approach reduces computational complexity and the generalized lack of data that can be used to explicitly model trees.

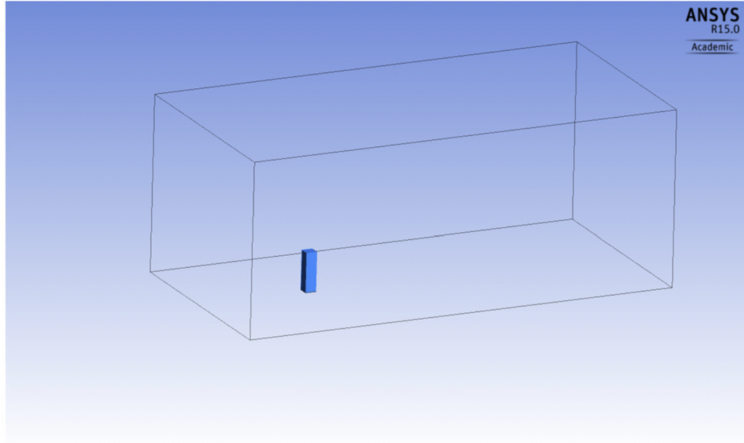


Figure 2.3: A single conifer modeled as a blue rectangular block, which was set as a porous zone (Source: Mohamed and Wood, 2015)

In this implicit tree modeling approach, tree drag is represented by adding a sink term (S_{ui}) in the momentum equation and source terms (S_k and S_ϵ) in the turbulence equations. Note that these sink/sources are only considered in porous zones that represent trees.

$$S_{ui} = -\rho C_d LAD U_i \mathbf{U} \left[\frac{N}{m^3} \right] \quad (2)$$

$$S_k = \rho C_d LAD (\beta_p \mathbf{U}^3 - \beta_d \mathbf{U}k) \left[\frac{W}{m^3} \right] \quad (3)$$

$$S_\epsilon = \rho C_d LAD \frac{\epsilon}{k} (C_{\epsilon 4} \beta_p \mathbf{U}^3 - C_{\epsilon 5} \beta_d \mathbf{U}k) \left[\frac{W}{m^3} \right] \quad (4)$$

where (2) is the sink term for the momentum equation, (3) is the source term for the turbulence kinetic energy equation, and (4) is the source term for the turbulent dissipation rate equation; ρ is the air density, C_d is the leaf drag coefficient, LAD is the leaf area density, U_i is the velocity component in direction i , \mathbf{U} is the wind speed magnitude, β_p is the fraction of mean kinetic energy converted into turbulent kinetic energy, β_d is the dimensionless coefficient for

the short-circuiting of turbulent cascade, $C_{\varepsilon 4}$ and $C_{\varepsilon 5}$ are model constants. Depending on the studied cases, several values for β_p , β_d , $C_{\varepsilon 4}$ and $C_{\varepsilon 5}$ could be found in the literature (Hong et al., 2018a; Hefny Salim et al., 2015; Santiago et al., 2019; Buccolieri et al., 2018; Liang et al., 2006). Usually, β_p is assumed equal to 1 and the values for β_d , $C_{\varepsilon 4}$ and $C_{\varepsilon 5}$ range between 4–6.5, 0.9–2 and 0.9–1.8, respectively (Buccolieri et al., 2018).

C_d is known to depend on tree species. In the literature, the values for C_d vary between 0.1 and 0.3, with 0.2 being the most commonly used (Gromke et al., 2015). LAD , defined as the one-side leaf surface area per unit volume ($m^2 m^{-3}$) (5), also depends on tree species and varies with height over the tree crown. The values used in CFD simulations range from 0.1 to 4, with an average value in the literature about 1 (Buccolieri et al., 2018). For deciduous trees, the effect of seasons can also lead to variation in LAD values. Lalic and Mihailovic (2004) reported LAD values for deciduous trees ranging from 0.2 to 2.2, where 1.6, 2.0 and 2.2 are the respective maximum values of LAD for the canopy of full grown oak, silver birch and maple trees.

$$LAD = \frac{A_{leaf}}{V} \quad (5)$$

The Leaf Area Index (LAI), the ratio of the leaf area to the ground area ($m^2 m^{-2}$), describes the tree density and its relationship with LAD is defined as:

$$LAI = \int_z^h LAD(z) dz \quad (6)$$

where h is the height of the tree. LAI values of several types of trees are discussed in Parker (2020). The mean values for LAI of broadleaf and conifer trees are $4.02(\pm 2.44)$ and $5.18(\pm 3.22)$, respectively (Parker, 2020). For trees with known LAI , the LAD values can be obtained from the generalised canopy density curves defined in the literature (Shaw and Schumann, 1992; Von Der Grün et al., 2020). Figure 2.4 shows the $LAD - LAI$ model defined by Von Der Grün et al. (2020), where $LAI = 2$ represents a sparsely covered tree canopy in winter and $LAI = 5$ a very dense tree canopy in summer.

In addition, there have been studies that provide methods to acquire LAD and LAI values from airborne LiDAR data (Oshio et al., 2015; Kamoske et al., 2019). These methods usually voxelize LiDAR point clouds, and then estimate LAD and LAI values based on the information of each voxel, e.g., number of returns. Yet the applicability of these methods in CFD simulations remains to be investigated.

2.3 Automatic Reconstruction of Trees

With the development of 3D tree reconstruction methods, some studies have also attempted to use real tree models instead of porous zones in CFD simulations. For example, Wang et al. (2021) used a deciduous tree model with tree trunks and branches to simulate the dispersion of pollutants in a street canyon. However, even though the model contained only one tree, the mesh cells have reached more than two million. This means that a detailed tree model like this is too demanding for a street or city scale application covering multiple buildings and trees. For such larger scale applications, it is necessary to reduce LoDs of tree models.

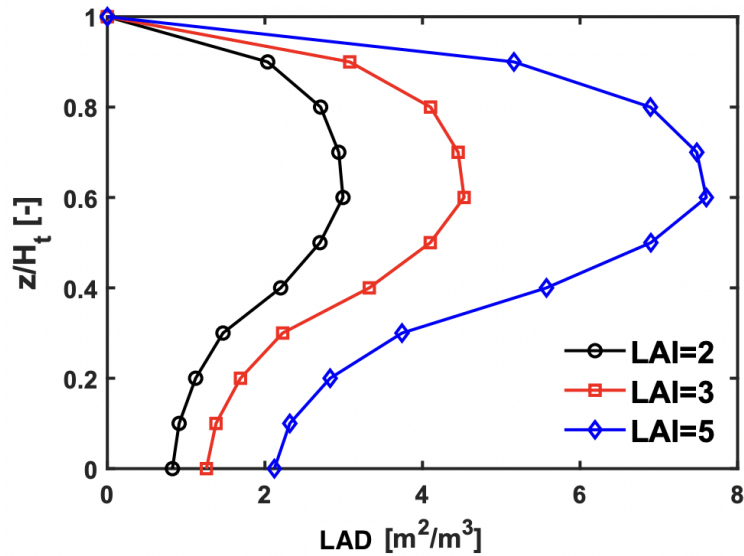


Figure 2.4: Profiles of LAD over the dimensionless tree height H_t for different LAI . (Source: Von Der Grün et al., 2020)

There are existing standards or proposed standards for LoDs of 3D tree models. Liang et al. (2016) introduced 5 LoDs for single tree reconstruction, as shown in figure 2.5. Based on this, Ortega-Córdova (2018) further proposed 14 LoDs (figure 2.6) to meet the requirements of different research cases and scales.

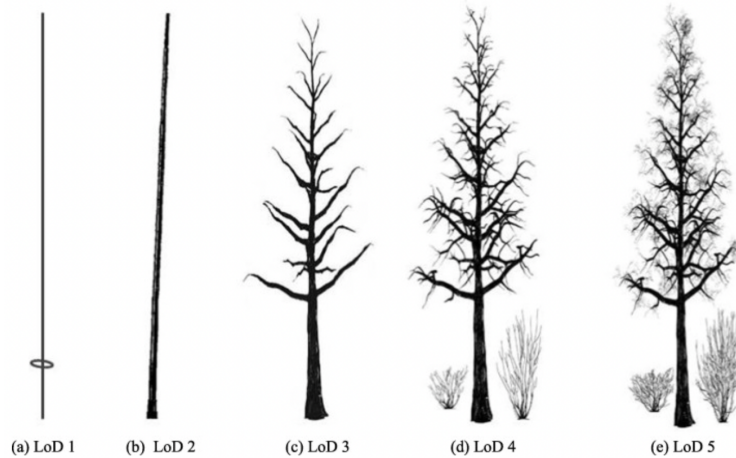


Figure 2.5: Levels of details of a single 3D tree model. (Source: Liang et al., 2016)

Making use of the proposed LoD specifications by Ortega-Córdova (2018), de Groot (2020) offered an automatic reconstruction of trees in different LoDs, as shown in figure 2.7 and 2.8. The LoD1 models obtained by this method are cylindrical or prismatic, which are similar in shape to the tree models used to obtain porous zones in many current studies (figure 2.3). Tree models in LoD2 or higher are mainly composed of a crown and a trunk, and they differ mainly in the fineness of the crown. It is worth mentioning that de Groot (2020) also classified trees into two groups, Coniferae and Angiospermae, and this information is stored as an attribute in each tree model.

Other works have focused on providing highly detailed tree reconstruction methods (Du et al.,

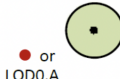
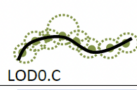
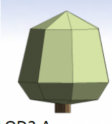
	LODx.A	LODx.B	LODx.C	LODx.D
LOD0.x	 • or LOD0.A	 LOD0.B	 LOD0.C	
LOD1.x	 LOD1.A	 LOD1.B	 LOD1.C	 LOD1.D
LOD2.x	 LOD2.A	 LOD2.B	 LOD2.C	
LOD3.x	 LOD3.A	 LOD3.B	 LOD3.C	 LOD3.D

Figure 2.6: Levels of details of a single 3D tree model. (Source: Ortega-Córdova, 2018)

(2019; Livny et al., 2011), which results in tree models that include not only trunks and crowns, but also fine branches and leaves. However, such models are usually too complex to be applicable to CFD simulations. Moreover, as presented by Du et al. (2019), highly detailed tree reconstruction models often require LiDAR point cloud data from mobile scanning or static scanning, which are difficult to obtain, so they are therefore not applicable to most urban wind environment studies. Hence, it can be safely concluded that these highly detailed tree models are beyond the scope of this thesis.

García-Sánchez et al. (2021) have demonstrated that different LoDs lead to diverse local numerical wind predictions by comparing CFD simulations results with building models in different LoDs. However, to my knowledge, few studies have given extensive consideration to the tree LoD impact on urban wind flow simulations, which will be one of the research focuses of this thesis.

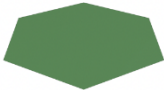
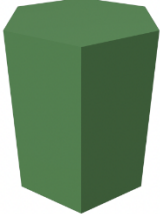
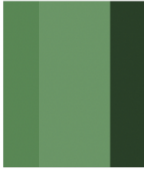
	3D view	Front View	Top View
LOD ₀			
LOD ₁			
LOD ₂			
LOD _{3.0}			
LOD _{3.1}			

Figure 2.7: Tree models with different LoDs by [de Groot \(2020\)](#).



Figure 2.8: LoD2 tree models by [de Groot \(2020\)](#).

3 Research questions

The main research question for this thesis is:

what is the impact of tree topology modelling for urban flow simulations?

To answer this, the following sub-questions will be relevant:

- How to obtain implicit tree models and explicit tree models from point cloud?
- How to extract related parameters from point cloud?
- How to design ideal numerical test cases to better compare simulation results?
- What is the difference between simulation results using current implicit tree models and explicit tree models?
- What is the tree LoD impact on urban wind flow simulations?
- Based on the comparison of implicit and explicit tree models, can we provide improvements in traditional drag approaches?

3.1 Scope of research

This thesis focuses on design numerical test cases and comparisons between simulation results, and will not work on building completely new tree reconstruction algorithms. In order to obtain tree models of different shapes and LoD from open point cloud data, this thesis will find suitable tree reconstruction algorithms among the already existing ones to be used directly or with minor changes to fit CFD applications. The algorithm introduced by [de Groot \(2020\)](#) will be mainly applied and adapted, and if necessary, the algorithm provided by [Zhu et al. \(2008\)](#) will also be considered.

4 Methodology

Methodology of this thesis can be divided into three main parts:

1. Numerical test case designs
2. 3D models preparation
3. CFD simulations and results analysis

Figure [4.1](#) displays a general workflow of this thesis. First, a series of ideal numerical test cases with trees of different shapes and LoDs and with different surrounding building arrangements will be designed. These designs will be applied in both implicit and explicit approach. Based on these designs, 3D building models need to be prepared and tree models in different LoDs will be reconstructed using open 3D point cloud data. Also, parameters useful for the implicit approach, such as tree height and *LAD*, will be extracted from the point cloud data. Then, the reconstructed tree models will be used to obtain implicit and explicit CFD models that have as similar mesh design as possible. Finally, the simulation results of the two approaches under different case designs will be compared in terms of velocity magnitude, turbulent kinetic energy, and pedestrian wind comfort. The insights gathered will be used to evaluate the per-

formance of traditional drag approaches and explore the potential improvements in implicit tree modelling using the explicit tree models as a reference.

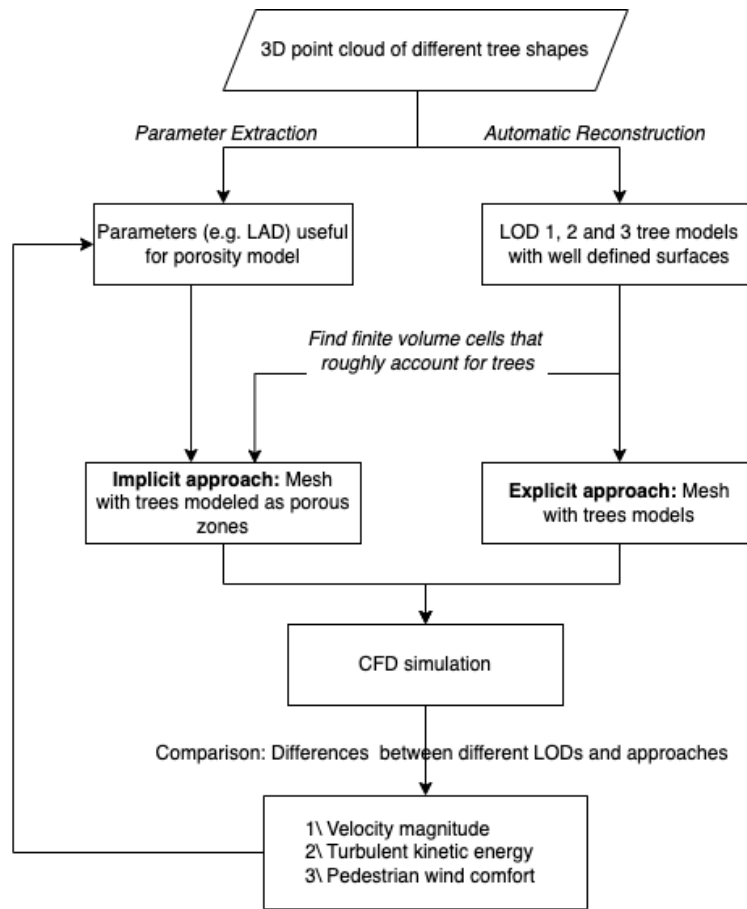


Figure 4.1: Methodology

4.1 Numerical test case designs

The purpose of this step is to design suitable test cases in order to cover the different geometrical complexity of urban areas and better analyze impact of tree topology modelling for urban flow simulations. Illuminating cases settings can be found in some literature (Hefny Salim et al., 2015; Vos et al., 2013). Hefny Salim et al. (2015) considered three morphologies: an idealized street canyon, a simplified urban geometry (array of buildings), and a realistic urban geometry. In this way, tree effects in CFD applications at different scales can be more fully understood. Whereas Vos et al. (2013) only considered the street canyon scale, and 19 different green streets designed by urban planners were considered in the case studies (figure 4.2). All 19 designs were believed by the designers to improve air quality and were actually implemented in real projects. Yet, only in one design (case 4) was a significant air quality improvement observed.

Considering the research objectives of this thesis, I tentatively believe that two scales of test cases are necessary: the street canyon and a realistic urban geometry. The main components of each test case are building and tree models, where tree models are reconstructed in LoD1, 2 and 3. For tree types, at least Coniferous and Broadleaf trees will be considered. Since most of the deciduous trees are broadleaf and only very few coniferous trees are deciduous

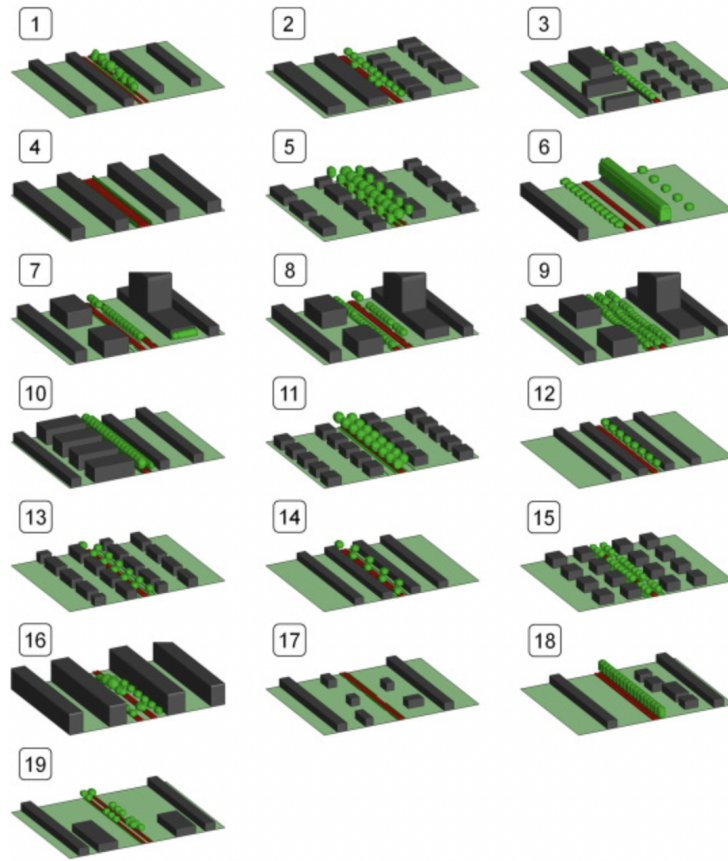


Figure 4.2: Green street designs for the case studies in Vos et al. (2013)

(Wikipedia, 2021), the effect of seasons will only be considered in broadleaf trees.

The street canyon scale test cases were used primarily to analyze the local changes in wind flow due to the effects of tree topography modeling, such as changes in the rotating vortex within the canyon and the airflow above the tops of buildings. The insights obtained can be used to analyze the further effects of tree topography on pollutant dispersion and heat exchange. On the other hand, the test cases using a realistic urban geometry are mainly used to simulate more complex tree effects on the airflow. Complicated street and tree configurations and variations in building shapes result in more complicated flow fields, which allow the effects of tree topology modeling to potentially no longer be confined to local areas. The insights obtained may be important for larger-scale studies of urban wind environments.

4.1.1 Street canyon

For the street canyon scale, at least two street configurations will be considered: 1) street length $L = 180m$, building height $H = 18m$, with an aspect ratio (street width W to H) of 1; 2) the same values for L and H but with an aspect ratio of 2. Based on these two street configurations, the variables of the tree configurations will include the types and LoDs of trees (i.e., with different shapes and parameters) and the number of trees (one or two rows). Also, both treatments of trees effects, i.e. the implicit approach and explicit approach, are taken into account. The settings of simulation cases that have been designed so far are summarized in table 1. Note that only test cases using the implicit approach are listed in this table. Test cases

Table 1: Test cases using the implicit approach for the street canyon

ID	Treatment of trees effect	Street configuration	Tree configurations	Season
1	Implicit approach	Aspect ratio W/H = 1	One row trees, LoD1, Coniferous trees	Summer
2			One row trees, LoD2, Coniferous trees	
3			One row trees, LoD3, Coniferous trees	
4			One row trees, LoD1, Broadleaf trees	
5			One row trees, LoD2, Broadleaf trees	
6			One row trees, LoD3, Broadleaf trees	
7			One row trees, LoD1, Broadleaf trees	Winter
8			One row trees, LoD2, Broadleaf trees	
9			One row trees, LoD3, Broadleaf trees	
10		Aspect ratio W/H = 2	Two row trees, LoD1, Coniferous trees	Summer
11			Two row trees, LoD2, Coniferous trees	
12			Two row trees, LoD3, Coniferous trees	
13			Two row trees, LoD1, Broadleaf trees	
14			Two row trees, LoD2, Broadleaf trees	
15			Two row trees, LoD3, Broadleaf trees	
16			Two row trees, LoD1, Broadleaf trees	Winter
17			Two row trees, LoD2, Broadleaf trees	
18			Two row trees, LoD3, Broadleaf trees	

using the implicit approach will use the same street, tree, and season configuration, so there are 36 test case designs in total. I will continue to analyze the need for these current designs, and if possible, will reduce the total case number to less than 20.

4.1.2 Realistic urban geometry

For the realistic urban geometry, I plan to use a LOD1.3 city model of a part of the Delft University of Technology campus (figure 4.3) that can be obtained through the 3D BAG database (Dukai et al., 2021). Trees in the domain will be classified as either coniferous or broadleaf. The differences between the test cases are mainly in the seasons, the LoDs of tree models and the treatments of tree effects, as shown in table 2

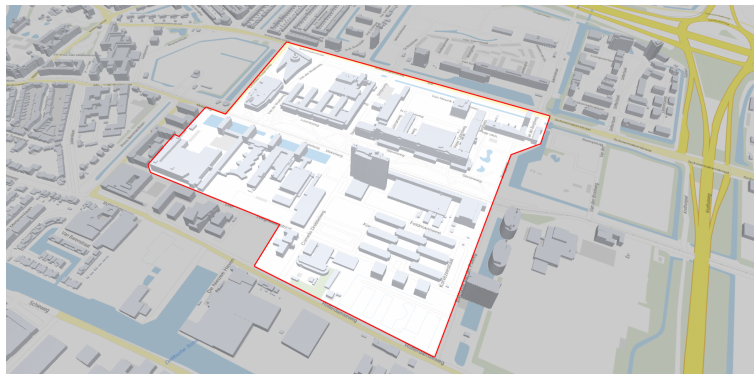


Figure 4.3: LoD1.3 model shown in the 3D BAG database; The red line represents the expected research area

4.2 3D models preparation

This step focuses on the preparation of building and tree models for each numerical test case.

Table 2: Test cases for the realistic urban geometry

ID	Treatment of trees effect	Tree configurations	Season
1	Implicit approach	LoD1	Summer
2		LoD2	
3		LoD3	
4		LoD1	Winter
5		LoD2	
6		LoD3	
7	Explicit approach	LoD1	Summer
8		LoD2	
9		LoD3	
10		LoD1	Winter
11		LoD2	
12		LoD3	

4.2.1 Street canyon

In each street canyon considered in these test cases, two building models of $180m$ in length, $20m$ in width and $18m$ in height, and perpendicular to the approaching wind direction, were required. The building models can be created with Blender, a free and open source 3D creation suite. Figure 4.4 shows an example of a street canyon with an aspect ratio of 2 that I have created with Blender.

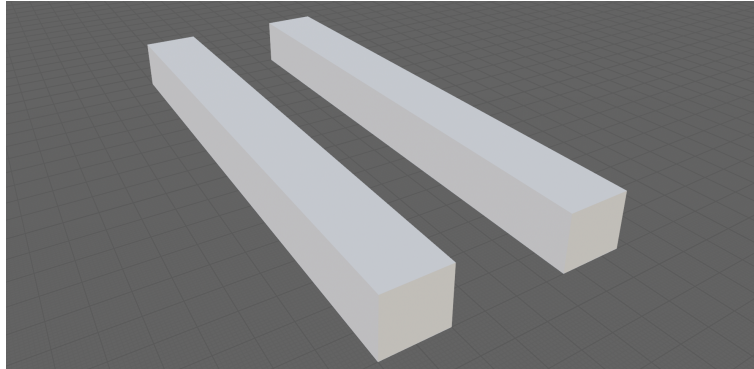


Figure 4.4: Examples of a street canyon with an aspect ratio of 2

Tree models, as mentioned earlier, will include at least two types: Coniferous and Broadleaf trees. In this group of test cases, a coniferous tree scale model and a broadleaf tree scale model, both with relatively standard shapes, will be used. These two tree models can be obtained by point cloud segmentation, classification, reconstruction. Figure 4.5 shows the two LoD2 tree models that I have obtained using the AHN3 point cloud dataset and the automatic reconstruction algorithm adapted from de Groot (2020), which are classified as a broadleaf and a coniferous tree, respectively.

Values of the drag coefficient C_d for these two tree models will be defined as a constant, which is consistent with most of the literature. For LAD , two values are needed for the broadleaf tree model, for the dense foliage in summer and the sparse foliage in winter. The conifer tree model, on the other hand, requires only one LAD value. I will refer to the work of (Buccolieri et al., 2018; Lalic and Mihailovic, 2004; Parker, 2020; Von Der Grün et al., 2020) mentioned in section 2.2 to find the appropriate LAD values for these two tree models.

Moreover, I will continue to search for available open tree point cloud data in order to get more tree models for coniferous and broadleaf trees respectively. For example, for broadleaf trees, i.e. deciduous trees, I expect to obtain one tree model each for oak, maple, and birch, ideally with significant differences in shape and height. This allows me to study the effect of tree topology on wind in a more detailed way.

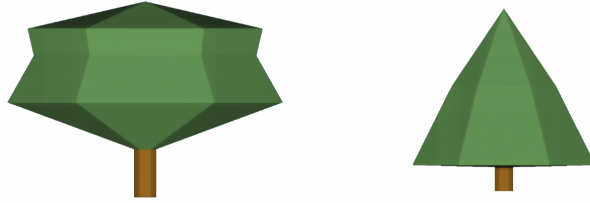


Figure 4.5: Examples of a LoD2 broadleaf tree (left) and a LoD2 coniferous tree (right)

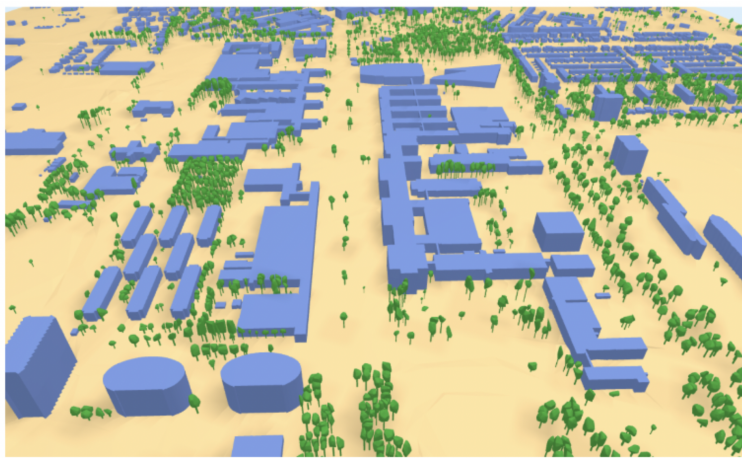


Figure 4.6: TUDelft campus model with LoD2 tree models

4.2.2 Realistic urban geometry

The building models for this group of test cases are consistent, i.e. the LoD1.3 building models from the 3D BAG database (Dukai et al., 2021).

The LoD1, 2 and 3 tree models will be obtained using the AHN3 point cloud dataset and the reconstruction algorithm adapted from (de Groot, 2020). Each tree is classified as either a conifer or a broadleaf tree. Figure 4.6 shows an example of the TUDelft campus model with LoD2 tree models that I have created.

Similar to the street canyon test cases, values of the drag coefficient C_d for these tree models will be defined as a constant. For estimating each tree's LAD value, I will first try to use the open-source LAD acquisition methods from point clouds, mentioned in section 2.2. Ideally, the LAD values would be used as a tabular data for CFD simulations. A simpler approach is to pre-define constant LAD values based on the literature, similar to what was done in the street canyon test cases.

4.3 CFD simulations and results analysis

To perform the CFD simulations, OpenFOAM, an open-source computational fluid dynamics software, is used. The flow is considered incompressible, steady and temperature stratification is neutral.

4.3.1 Governing equations

The Reynolds-averaged Navier-Stokes (RANS) approach is used for CFD simulations. The mass (7) and momentum conservation equations that govern the flow are the following:

$$\frac{\partial \bar{u}_j}{\partial x_j} = 0 \quad (7)$$

$$\bar{u}_j \frac{\partial \bar{u}_i}{\partial x_j} = -\frac{1}{\rho} \frac{\partial \bar{p}}{\partial x_i} + \nu \frac{\partial^2 \bar{u}_j}{\partial x_j \partial x_j} - \frac{\partial \overline{u'_i u'_j}}{\partial x_j} + F_i \quad (8)$$

where u_i denotes time-averaged velocity components, ρ is the density, p is the pressure, ν is the kinematic viscosity and F_i is the source or sink term. F_i is only considered in porous zones that represents trees and is equal to Equation 2. In other cases, it is zero. The term $\overline{u'_i u'_j}$ represents the Reynolds stress tensor, which is unknown and needs to be closed with a turbulence model. For our case, we used the two equations $k - \epsilon$ turbulence model since it is widely used in outdoor wind simulations, and it is rather simple (García-Sánchez et al., 2021; Blocken, 2015). In this model, $\overline{u'_i u'_j}$ is computed based on the linear eddy viscosity hypothesis:

$$\overline{u'_i u'_j} = \frac{2}{3} k \delta_{ij} - 2\mu_t S_{ij} \quad (9)$$

where k is the turbulence kinetic energy, S_{ij} the time-averaged shear stress tensor, and μ_t is the coefficient termed turbulence viscosity. μ_t is computed using following equation:

$$\mu_t = C_\mu \frac{k^2}{\epsilon} \quad (10)$$

where C_μ is a model constant equal to 0.09. The equations for the two turbulence variables, namely the turbulence kinetic energy k and the turbulence dissipation rate ϵ are as follows:

$$\bar{u}_j \frac{\partial k}{\partial x_j} = \frac{\partial}{\partial x_j} \left[\left(\mu + \frac{\mu_t}{\sigma_k} \right) \frac{\partial k}{\partial x_j} \right] + P_k - \epsilon \quad (11)$$

$$\bar{u}_j \frac{\partial \epsilon}{\partial x_j} = \frac{\partial}{\partial x_j} \left[\left(\mu + \frac{\mu_t}{\sigma_\epsilon} \right) \frac{\partial \epsilon}{\partial x_j} \right] + C_{\epsilon 1} \frac{\epsilon}{k} P_k - C_{\epsilon 2} \frac{\epsilon^2}{k} \quad (12)$$

where P_k is the turbulent production term and σ_k , σ_ϵ , $C_{\epsilon 1}$ and $C_{\epsilon 2}$ are model constants, with values of 1.0, 1.3, 1.44, and 1.92, respectively.

4.3.2 Computational domain and mesh

For all numerical test cases, the computational domain should be chosen large enough to avoid too strong artificial acceleration of the flow due to too strong contraction of the flow by the side and top boundaries of the computational domain (Blocken, 2015). Conform to the best practice guidelines prescribed by Franke et al. (2011); Blocken (2015), the inlet, lateral and top boundary are set at least $5H_{max}$ away from the group of building and tree models, where $5H_{max}$ is the height of the tallest geometry. A distance of at least $15H_{max}$ should be kept downstream of the group of building and tree models to allow for adequate wake development.

For generating the computational mesh, i.e., to discretize the space where the airflow is modelled, the automatic parallel mesh generator *snappyHexMesh* is used. An example of the computational mesh design for a single tree model is shown in figure 4.7. It can be seen that the cell density increases closer to the ground and to the tree. Note that in order to ensure the comparability of CFD predictions, the test cases to be compared should use computational mesh designs that are as similar as possible. Figure 4.8 shows the computational meshes I designed for a test case using the implicit approach for tree modelling and a test case using the explicit approach, respectively. It can be found that the two meshes are overall consistent, except that the explicit approach test case has no cells within the tree model, while in the test case using the implicit approach, these cells are still present, marked as porous zones.

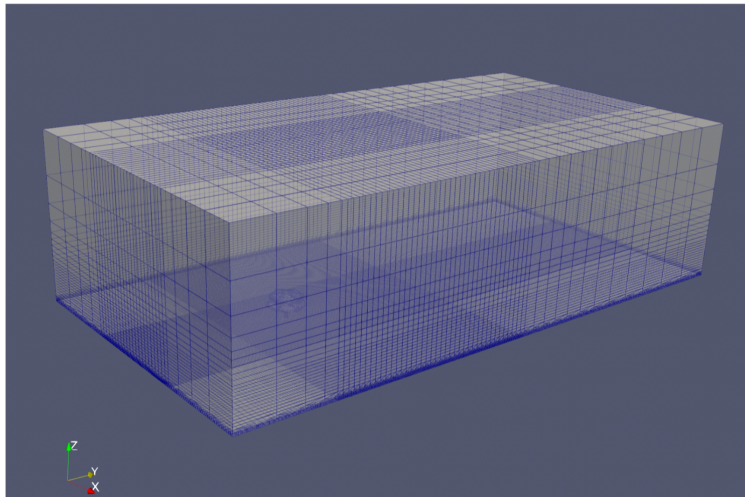


Figure 4.7: Planning overview

4.3.3 Boundary conditions

For each test case, the same meteorological conditions will be used: the inlet wind speed is 4.97 m/s at 10 m above the ground. The inflow boundary condition will be modelled as a fully-developed neutral boundary condition with the following equations for the velocity, turbulence kinetic energy, and dissipation:

$$U = \frac{u_*}{\kappa} \ln \frac{z + z_0}{z_0} \quad (13)$$

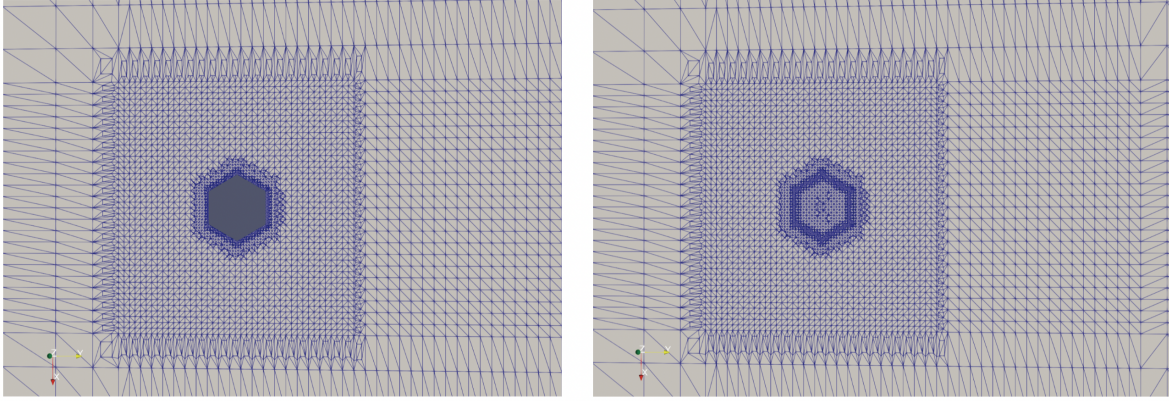


Figure 4.8: the computational mesh designs (Horizontal cross-section) for a test case using the explicit approach for tree modelling (left) and a test case using the implicit approach (right).

$$k = \frac{u_*^2}{\sqrt{C_\mu}} \quad (14)$$

$$\epsilon = \frac{u_*^3}{\kappa(z + z_0)} \quad (15)$$

where u_* denotes the friction velocity, z_0 is the aerodynamic roughness length and κ is the von Karman constant with a value of 0.41.

To run the simulation, the *simpleFoam* solver will be used, with blended second order discretization schemes. Figure 4.9 shows the preliminary simulation results for the two cases mentioned in section 4.3.2.

5 Time planning

Figure 5.1 gives an overview of the schedule set up for activities that are needed to achieve the research objectives. The exact dates for P3, P4 and P5 will be determined during the year.

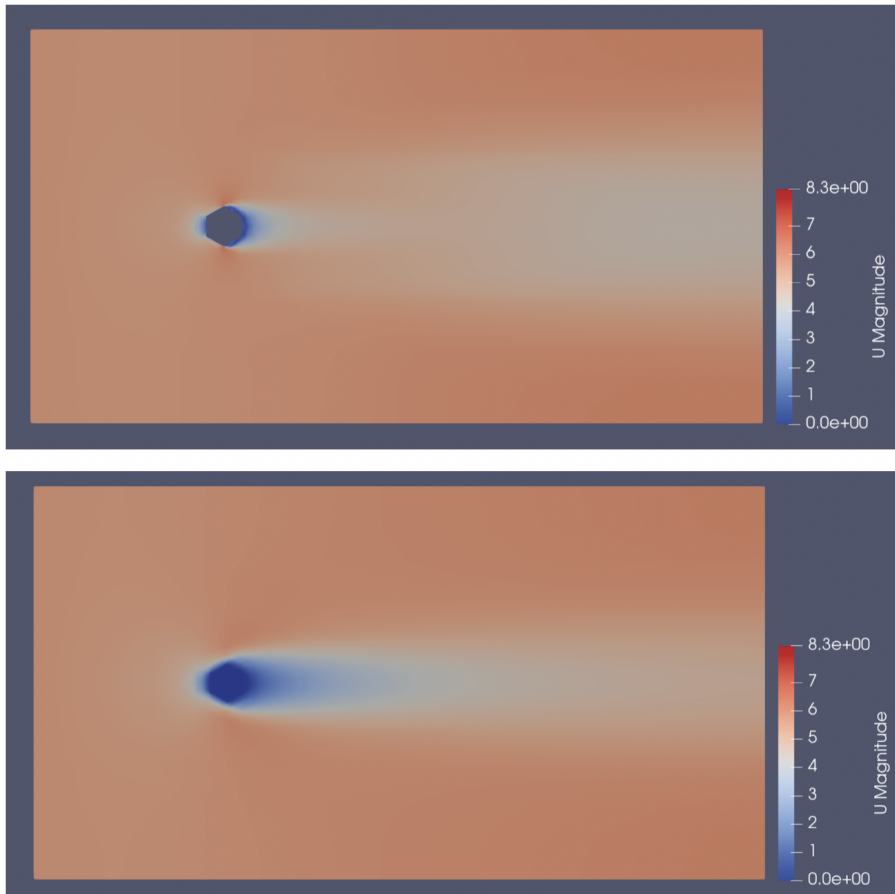


Figure 4.9: The CFD predictions (Horizontal cross-section) for a test case using the explicit approach (up) and a test case using the implicit approach (down).

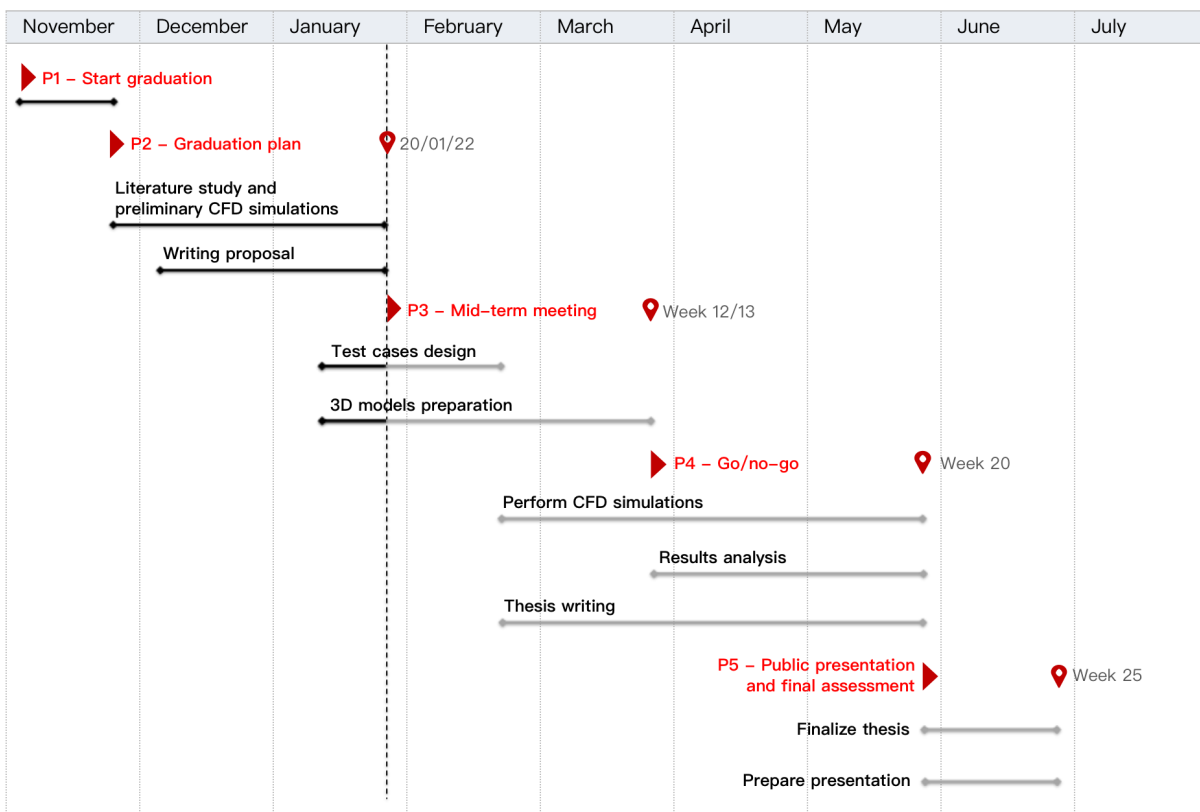


Figure 5.1: Planning overview

6 Tools and datasets used

Open point cloud datasets such as the *Actueel Hoogtebestand Nederland* (AHN3) dataset available at [PDOK](#) will be used to obtain tree models. To obtain the LoD1.3 city model of a part of the TUDelft campus, the 3D BAG database ([Dukai et al., 2021](#)) will be used. Also, the tree reconstruction algorithms introduced by [de Groot \(2020\)](#) is mainly applied and adapted in this thesis, and if necessary, the algorithm provided by [\(Zhu et al., 2008\)](#) will also be considered.

Table 3 lists the software, programming languages and other tools used or planned for use in this thesis.

Table 3: Tools used or planned for use

Software	Purpose
OpenFoam	Perform CFD simulations
Paraview	Post-processing & visualization
Meshlab	Visualisation
Blender	Create and Edit STL files
FME	Spatial data processing
Programming Languages	Purpose
C++	OpenFOAM implementations
Python	3D models preparation
Others	Purpose
PyVista	Automatic CFD post-processing with Python

References

- A. Aflaki, M. Mirnezhad, A. Ghaffarianhoseini, A. Ghaffarianhoseini, H. Omrany, Z. H. Wang, and H. Akbari. Urban heat island mitigation strategies: A state-of-the-art review on Kuala Lumpur, Singapore and Hong Kong. *Cities*, 62:131–145, 2 2017. ISSN 0264-2751. doi: 10.1016/J.CITIES.2016.09.003.
- M. Balczó, C. Gromke, and B. Ruck. Numerical modeling of flow and pollutant dispersion in street canyons with tree planting. *Meteorologische Zeitschrift*, 18(2):197–206, 2009. ISSN 09412948. doi: 10.1127/0941-2948/2009/0361.
- B. Blocken. Computational Fluid Dynamics for urban physics: Importance, scales, possibilities, limitations and ten tips and tricks towards accurate and reliable simulations. *Building and Environment*, 91:219–245, 9 2015. ISSN 0360-1323. doi: 10.1016/J.BUILDENV.2015.02.015.
- B. Blocken, W. D. Janssen, and T. van Hooff. CFD simulation for pedestrian wind comfort and wind safety in urban areas: General decision framework and case study for the Eindhoven University campus. *Environmental Modelling & Software*, 30:15–34, 4 2012. ISSN 1364-8152. doi: 10.1016/J.ENVSOFT.2011.11.009.
- R. Buccolieri, J. L. Santiago, E. Rivas, and B. Sanchez. Review on urban tree modelling in CFD simulations: Aerodynamic, deposition and thermal effects. *Urban Forestry & Urban Greening*, 31:212–220, 4 2018. ISSN 1618-8667. doi: 10.1016/J.UFUG.2018.03.003.
- R. de Groot. Automatic construction of 3D tree models in multiple levels of detail from airborne LiDAR data, 2020. URL <https://repository.tudelft.nl/islandora/object/uuid%3A3e169fc7-5336-4742-ab9b-18c158637cfe>.

- S. Du, R. Lindenbergh, H. Ledoux, J. Stoter, and L. Nan. AdTree: Accurate, Detailed, and Automatic Modelling of Laser-Scanned Trees. *Remote Sensing* 2019, Vol. 11, Page 2074, 11 (18):2074, 9 2019. ISSN 20724292. doi: 10.3390/RS11182074. URL <https://www.mdpi.com/2072-4292/11/18/2074/htmhttps://www.mdpi.com/2072-4292/11/18/2074>.
- B. Dukai, J. van Liempt, R. Peters, J. Stoter, S. Vitalis, and T. Wu. 3D BAG Viewer, 2021. URL <https://3dbag.nl/en/viewer>.
- A. Fouillet, G. Rey, F. Laurent, G. Pavillon, S. Bellec, C. Guihenneuc-Jouyaux, J. Clavel, E. Jouglà, and D. Hémon. Excess mortality related to the August 2003 heat wave in France. *International Archives of Occupational and Environmental Health*, 80(1):16–24, 10 2006. ISSN 03400131. doi: 10.1007/S00420-006-0089-4. URL https://www.researchgate.net/publication/7255542_Excess_Mortality_Related_to_the_August_2003_Heat_Wave_in_France.
- J. Franke, A. Hellsten, K. H. Schlunzen, and B. Carissimo. The COST 732 Best Practice Guideline for CFD simulation of flows in the urban environment: a summary. *International Journal of Environment and Pollution*, 44(1-4):419–427, 2011. doi: 10.1504/IJEP.2011.038443. URL <https://www.inderscienceonline.com/doi/abs/10.1504/IJEP.2011.038443>.
- C. García-Sánchez, S. Vitalis, I. Paden, and J. Stoter. The impact of level of detail in 3d city models for cfd-based wind flow simulations. *International Archives of the Photogrammetry, Remote Sensing and Spatial Information Sciences - ISPRS Archives*, 46(4/W4-2021):67–72, 10 2021. ISSN 1682-1750. doi: 10.5194/ISPRS-ARCHIVES-XLVI-4-W4-2021-67-2021. URL <https://research.tudelft.nl/en/publications/the-impact-of-level-of-detail-in-3d-city-models-for-cfd-based-win>.
- C. Gromke, B. Blocken, W. Janssen, B. Merema, T. van Hooff, and H. Timmermans. CFD analysis of transpirational cooling by vegetation: Case study for specific meteorological conditions during a heat wave in Arnhem, Netherlands. *Building and Environment*, 83:11–26, 1 2015. ISSN 0360-1323. doi: 10.1016/J.BUILDENV.2014.04.022.
- M. Hefny Salim, K. Heinke Schlünzen, and D. Grawe. Including trees in the numerical simulations of the wind flow in urban areas: Should we care? *Journal of Wind Engineering and Industrial Aerodynamics*, 144:84–95, 9 2015. ISSN 01676105. doi: 10.1016/J.JWEIA.2015.05.004. URL https://www.researchgate.net/publication/281102280_Including_trees_in_the_numerical_simulations_of_the_wind_flow_in_urban_areas_Should_we_care.
- B. Hong and B. Lin. Numerical studies of the outdoor wind environment and thermal comfort at pedestrian level in housing blocks with different building layout patterns and trees arrangement. *Renewable Energy*, 73:18–27, 1 2015. ISSN 0960-1481. doi: 10.1016/J.RENENE.2014.05.060.
- B. Hong, H. Qin, and B. Lin. Prediction of Wind Environment and Indoor/Outdoor Relationships for PM2.5 in Different Building–Tree Grouping Patterns. *Atmosphere* 2018, Vol. 9, Page 39, 9(2):39, 1 2018a. ISSN 20734433. doi: 10.3390/ATMOS9020039. URL <https://www.mdpi.com/2073-4433/9/2/39/htmhttps://www.mdpi.com/2073-4433/9/2/39>.
- S. W. Hong, L. Zhao, and H. Zhu. CFD simulation of airflow inside tree canopies discharged from air-assisted sprayers. *Computers and Electronics in Agriculture*, 149:121–132, 6 2018b. ISSN 0168-1699. doi: 10.1016/J.COMPAG.2017.07.011.
- C. M. Hsieh and H. C. Huang. Mitigating urban heat islands: A method to identify potential wind corridor for cooling and ventilation. *Computers, Environment and Urban Systems*, 57: 130–143, 5 2016. ISSN 01989715. doi: 10.1016/J.COMPENVURBSYS.2016.02.005.

- A. G. Kamoske, K. M. Dahlin, S. C. Stark, and S. P. Serbin. Leaf area density from airborne LiDAR: Comparing sensors and resolutions in a temperate broadleaf forest ecosystem. *Forest Ecology and Management*, 433:364–375, 2 2019. ISSN 0378-1127. doi: 10.1016/J.FORECO.2018.11.017.
- G. Kang, J. J. Kim, and W. Choi. Computational fluid dynamics simulation of tree effects on pedestrian wind comfort in an urban area. *Sustainable Cities and Society*, 56:102086, 5 2020. ISSN 2210-6707. doi: 10.1016/J.SCS.2020.102086.
- B. Lalic and D. Mihailovic. An Empirical Relation Describing Leaf-Area Density inside the Forest for Environmental Modeling. *Journal of Applied Meteorology - J APPL METEOROL*, 43: 641–645, 1 2004. doi: 10.1175/1520-0450(2004)043<0641:AERDLD>2.0.CO;2.
- L. Liang, L. Xiaofeng, L. Borong, and Z. Yingxin. Improved $k-\epsilon$ two-equation turbulence model for canopy flow. *Atmospheric Environment*, 40(4):762–770, 2 2006. ISSN 1352-2310. doi: 10.1016/J.ATMOENV.2005.10.010.
- X. Liang, V. Kankare, J. Hyyppä, Y. Wang, A. Kukko, H. Haggrén, X. Yu, H. Kaartinen, A. Jaakkola, F. Guan, M. Holopainen, and M. Vastaranta. Terrestrial laser scanning in forest inventories. *ISPRS Journal of Photogrammetry and Remote Sensing*, 115:63–77, 5 2016. ISSN 0924-2716. doi: 10.1016/J.ISPRSJPRS.2016.01.006.
- Y. Livny, S. Pirk, Z. Cheng, F. Yan, O. Deussen, D. Cohen-Or, and B. Chen. Texture-lobes for tree modelling. *ACM Transactions on Graphics*, 30(4):53, 7 2011. ISSN 07300301. doi: 10.1145/1964921.1964948. URL <https://cris.tau.ac.il/en/publications/texture-lobes-for-tree-modelling-2>.
- L. Manickathan, T. Defraeye, J. Allegrini, D. Derome, and J. Carmeliet. Parametric study of the influence of environmental factors and tree properties on the transpirative cooling effect of trees. *Agricultural and Forest Meteorology*, 248:259–274, 1 2018. ISSN 0168-1923. doi: 10.1016/J.AGRFORMET.2017.10.014.
- M. A. Mohamed and D. H. Wood. Computational study of the effect of trees on wind flow over a building. *Renewables: Wind, Water, and Solar 2015 2:1*, 2(1):1–8, 1 2015. ISSN 2198-994X. doi: 10.1186/S40807-014-0002-9. URL <https://link-springer-com.tudelft.idm.oclc.org/articles/10.1186/s40807-014-0002-9><https://link-springer-com.tudelft.idm.oclc.org/article/10.1186/s40807-014-0002-9>.
- M. Moradpour, H. Afshin, and B. Farhanieh. A numerical investigation of reactive air pollutant dispersion in urban street canyons with tree planting. *Atmospheric Pollution Research*, 8(2):253–266, 3 2017. ISSN 13091042. doi: 10.1016/J.APR.2016.09.002. URL https://www.researchgate.net/publication/308599202_A_numerical_investigation_of_reactive_air_pollutant_dispersion_in_urban_street_canyons_with_tree_planting.
- F. Moukalled, L. Mangani, and M. Darwish. Mathematical Description of Physical Phenomena. In *The Finite Volume Method in Computational Fluid Dynamics. Fluid Mechanics and Its Applications*, volume 113, pages 43–83. Springer, Cham, 2016. doi: 10.1007/978-3-319-16874-6{_}3. URL https://link-springer-com.tudelft.idm.oclc.org/chapter/10.1007/978-3-319-16874-6_3.
- L. Ortega-Córdova. Urban Vegetation Modeling 3D Levels of Detail, 2018. URL <https://repository.tudelft.nl/islandora/object/uuid:8b8967a8-0a0f-498f-9d37-71c6c3e532af?collection=education>.

- H. Oshio, T. Asawa, A. Hoyano, and S. Miyasaka. Estimation of the leaf area density distribution of individual trees using high-resolution and multi-return airborne LiDAR data. *Remote Sensing of Environment*, 166:116–125, 9 2015. ISSN 0034-4257. doi: 10.1016/J.RSE.2015.05.001.
- G. G. Parker. Tamm review: Leaf Area Index (LAI) is both a determinant and a consequence of important processes in vegetation canopies. *Forest Ecology and Management*, 477, 12 2020. ISSN 03781127. doi: 10.1016/J.FORECO.2020.118496.
- J. A. Salmond, M. Tadaki, S. Vardoulakis, K. Arbuthnott, A. Coutts, M. Demuzere, K. N. Dirks, C. Heaviside, S. Lim, H. MacIntyre, R. N. McInnes, and B. W. Wheeler. Health and climate related ecosystem services provided by street trees in the urban environment. *Environmental Health: A Global Access Science Source*, 15, 2016. ISSN 1476069X. doi: 10.1186/S12940-016-0103-6.
- J. L. Santiago, R. Buccolieri, E. Rivas, H. Calvete-Sogo, B. Sanchez, A. Martilli, R. Alonso, D. Elustondo, J. M. Santamaría, and F. Martin. CFD modelling of vegetation barrier effects on the reduction of traffic-related pollutant concentration in an avenue of Pamplona, Spain. *Sustainable Cities and Society*, 48:101559, 7 2019. ISSN 2210-6707. doi: 10.1016/J.SCS.2019.101559.
- R. H. Shaw and U. Schumann. Large-eddy simulation of turbulent flow above and within a forest. *Boundary-Layer Meteorology*, 61(1-2):47–64, 10 1992. ISSN 00068314. doi: 10.1007/BF02033994. URL https://www.researchgate.net/publication/225010714_Large-Eddy_Simulation_of_Turbulent_Flow_above_and_within_a_Forest.
- F. Szkordilisz and A. Zöld. Effect of Vegetation on Wind-Comfort. *Applied Mechanics and Materials*, 824:811–818, 1 2016. ISSN 1662-7482. doi: 10.4028/WWW.SCIENTIFIC.NET/AMM.824.811. URL <https://www-scientific-net.tudelft.idm.oclc.org/AMM.824.811>.
- Y. Tominaga, A. Mochida, R. Yoshie, H. Kataoka, T. Nozu, M. Yoshikawa, and T. Shirasawa. AIJ guidelines for practical applications of CFD to pedestrian wind environment around buildings. *Journal of Wind Engineering and Industrial Aerodynamics*, 96(10-11):1749–1761, 10 2008. ISSN 0167-6105. doi: 10.1016/J.JWEIA.2008.02.058.
- M. Von Der Grün, P. Zamre, Y. Chen, T. Lutz, U. Voß, and E. Kramer. Numerical study and LiDAR based validation of the wind field in urban sites. *Journal of Physics: Conference Series*, 1618(4), 9 2020. ISSN 17426596. doi: 10.1088/1742-6596/1618/4/042009. URL https://www.researchgate.net/publication/345327822_Numerical_study_and_LiDAR_based_validation_of_the_wind_field_in_urban_sites.
- P. E. Vos, B. Maiheu, J. Vankerkom, and S. Janssen. Improving local air quality in cities: To tree or not to tree? *Environmental Pollution*, 183:113–122, 12 2013. ISSN 0269-7491. doi: 10.1016/J.ENVPOL.2012.10.021.
- L. Wang, J. Su, Z. Gu, and L. Tang. Numerical study on flow field and pollutant dispersion in an ideal street canyon within a real tree model at different wind velocities. *Computers and Mathematics with Applications*, 81:679–692, 2021. doi: 10.1016/j.camwa.2019.12.026. URL <https://doi.org/10.1016/j.camwa.2019.12.026>.
- Wikipedia. Broad-leaved tree, 7 2021. URL https://en.wikipedia.org/wiki/Broad-leaved_tree.
- C. Zhu, X. Zhang, B. Hu, and M. Jaeger. Reconstruction of tree crown shape from scanned data. *Lecture Notes in Computer Science (including subseries Lecture Notes in Artificial Intelligence and Lecture Notes in Bioinformatics)*, 5093 LNCS:745–756, 2008. ISSN 03029743. doi:

10.1007/978-3-540-69736-7{_}79. URL https://www.researchgate.net/publication/221247492_Reconstruction_of_Tree_Crown_Shape_from_Scanned_Data.